A Study on Realization of Combined Amplitude and Phase Modulation Employing Elliptical Signals

Chunyi SONG

*Global Information and Telecommu-
nication Institute, Waseda Univ., Japan
song@aoni.waseda.jp*

Shigeru SHIMAMOTO

*Graduate School of Global Information and Tele-
communication Studies, Waseda Univ., Japan
shima@waseda.jp*

Abstract

In this paper, we investigate a new solution for combined amplitude and phase modulation, which is realized by employing elliptical signals. Signal characteristics of the proposed schemes are analyzed and then detection methods are investigated. The derived closed-form BER approximations, i.e. theoretical analysis results, are shown to be in agreement with simulation results. Furthermore, both results show that proposed schemes can achieve better noise performance than conventional schemes, and that the proposed schemes have flexibility to make trade-offs between power efficiency and bandwidth efficiency by varying eccentricity.

1. Introduction

Owing to the high spectral efficiency, quadrature amplitude modulation (QAM), especially 16QAM, have been intensively studied in 1990's [1]-[9]. Two types of 16QAM have shown advantages in different applications. 16QAM of square mapping (16 Square-QAM) has better power efficiency while 16QAM of star mapping (16 Star-QAM) is more attractive in mobile radio communication.

By employing elliptical carriers, some modulation schemes generally defined as Elliptical Modulation Schemes (EMSs), were proposed and investigated in our previous works [10]-[14]. Compared to conventional modulation schemes, EMSs have shown some attractive characteristics, among which we particularly notice that by varying eccentricity, EMSs can flexibly make trade-offs between bandwidth efficiency and power efficiency.

In this paper, we aim to realize combined amplitude and phase modulation by employing elliptical signals. The proposed 16-ary schemes are defined as 16-ary Elliptical Amplitude Phase Modulation (16-EAPM). Similar with 16QAM, according to the characteristics of signal constellation, two types of 16-EAPM are defined as 16 Square-EAPM and 16 Star-EAPM respectively.

Rest of this paper is organized as follows. Characteristics of 16-EAPM signals are derived and analyzed in sect.2; demodulation methods of 16-EAPM signals are discussed in sect.3; closed-form BER approximations are derived in sect.4; simulations are carried out and the achieved results are compared with analytical results in sect.5; finally the paper is concluded in sect.6.

2. Signal Characteristics of 16-EAPM

2.1. Signal Expression

General expressions of 16-EAPM signals are given by

$$\begin{aligned}
s(t) &= a \cdot R(t, e_c, \varphi_j) \cos(\omega_c t + \alpha_i + \varphi_j) \\
&= a \cdot R(t, e_c, \varphi_j) \cos(\omega_c t + \theta_k)
\end{aligned} \qquad , \tag{1}$$

as shown in Fig.1, a is semi-major axis, which also denotes signal amplitude; e_c is eccentricity, α_i is offset inclination angle of an ellipse, φ_j is phase defined based on major-axis of the ellipse and we call it major-axis-based phase; θ_k is signal phase and $\theta_k = \alpha_i + \varphi_j$ (i, j and k are integers); $R(t, e_c, \varphi_j)$ denotes an elliptical radius normalized by semi-major axis and its expression is given by

$$R(t, e_c, \varphi_j) = \sqrt{\frac{1 - e_c^2}{1 - e_c^2 \cos^2(\omega_r t + \varphi_j)}} \quad , \tag{2}$$

where ω_r is revolution angular frequency of elliptical radius, and the elliptical signals used in this paper are generated by setting same value for ω_r and carrier angular frequency ω_c.

For M-EPSK defined in [11], φ_j is equal to either of 0 and π, then (2) is simplified to

$$R(t, e_c) = \sqrt{\frac{1 - e_c^2}{1 - e_c^2 \cos^2(\omega_r t)}} \quad , \tag{3}$$

and accordingly, (1) is simplified to

$$s(t) = a \cdot R(t, e_c) \cdot \cos(\omega_c t + \theta_k) \quad . \tag{4}$$

In M-EAPM, amplitude variations are achieved by varying semi-major axis of the ellipse. Then M-EAPM signals can be generally expressed as:

$$s(t) = a_n \cdot R(t, e_c) \cos(\omega_c t + \theta_k) , \tag{5}$$

where a_n (n is an integer) is semi-major axis and which also denotes distance between constellation point and centre point; definitions of other variables are referred to (1) and (2).

To show the characteristics that elliptical signals are used as transmission carriers in M-EPSK, in [11], we illustrated constellations of M-EPSK based on ellipses. Similarly, in Fig.2 and Fig.3, we demonstrate constellations of two types of 16-EAPM based on ellipses.

In Fig.3, R and r denote outer ring and inner ring respectively, and $R = a_1$, $r = a_2$. Let β denote the ring ratio (outer ring to inner ring), according to [3], optimum β is equal to

$$\beta = \frac{R}{r} = \frac{4.61}{2.61} \approx 1.77 \quad . \tag{6}$$

Firstly, we derive signal expressions of 16-EAPM based on their initial definitions of combined amplitude and phase modulations. In 16 Square-EAPM, as shown in Fig.4, ellipses can be divided into three groups according to their values of semi-major axis, and signal phase θ equals to offset inclination angle of α. Accordingly, signal expressions are derived by substituting combinations of semi-major axis and signal phase to (5)

$$s(t) = a_n \cdot R(t, e_c) \cos(\omega_c t + \theta_k) = \tag{7}$$

$$\begin{cases} n = 1, \ a_1 \cdot R(t, e_c) \cos[\omega_c t + (2i - 1)\pi/4] & i = 1, 2, 3, 4 \\ n = 2, \ a_2 \cdot R(t, e_c) \cos[\omega_c t + f(i) \cdot \pi/4 + (-1)^i \cdot \varphi] & i = 1, 2, \ldots 8 \\ n = 3, \ a_3 \cdot R(t, e_c) \cos[\omega_c t + (2i - 1)\pi/4] & i = 1, 2, 3, 4 \end{cases} ,$$

where $f(i)$ and φ are given by

$$\begin{cases} f(i) = i - 3/2 - (-1)^i/2 \\ \varphi = \arcsin(1/\sqrt{10}) \end{cases} , \tag{8}$$

and without losing a generality, we define $a_3 > a_2 > a_1$.

In 16 Star-EAPM, ellipses have two values of semi-major axis and signal space is equally

partitioned into 8 regions, then signal expression is given by

$$
\begin{aligned}
s(t) &= a_n R(t, e_c) \cos(\omega_c t + \theta_k) \\
&= a_n R(t, e_c) \cos[\omega_c t + (2k-1)\pi/8] \quad ,
\end{aligned}
\tag{9}
$$

where n=1,2; k=1,2,…8.

Based on (7) and (9), general expressions of 16-EAPM signals can be given by:

$$
\begin{aligned}
s(t) &= a_n \cdot R(t,e_c)\cos(\omega_c t + \theta_k) = a_n\cos\theta_k \cdot R(t,e_c)\cdot\cos(\omega_c t) - a_n\sin\theta_k \cdot R(t,e_c)\cdot\sin(\omega_c t) \\
&= a_I \cdot \underbrace{R(t,e_c)\cdot\cos(\omega_c t)}_{C_{EI}} - a_Q \cdot \underbrace{R(t,e_c)\cdot\sin(\omega_c t)}_{C_{EQ}} \quad ,
\end{aligned}
\tag{10}
$$

where

$$
a_n = \sqrt{a_I^2 + a_Q^2} \quad ,
\tag{11}
$$

here, a_I and a_Q denote amplitudes of in-phase and quadrature phase components, respectively; definitions of the other variables are referred to (1); C_{EI} and C_{EQ} are orthogonal to each other.

16QAM modulated signals generally are given by

$$
s(t) = A_I \cos(\omega_c t) - A_Q \cdot \sin(\omega_c t) \quad ,
\tag{12}
$$

where A_I and A_Q are signal amplitudes of in-phase and quadrature phase components, respectively; ω_c represents carrier angular frequency [15].

Orthogonal signals of C_{EI} and C_{EQ} are used as transmission carriers in 16-EAPM. Then from (10) and (12), we know that 16-EAPM signals can be derived from 16QAM signals by replacing sinusoid carriers with elliptical carriers.

2.2. Frequency Spectrum

Frequency spectrums of 16-EAPM are calculated using Maple and MATLAB [16]. In comparison with 16QAM, extra two variables of eccentricity and signal phase might influence frequency spectrums in 16-EAPM. To investigate influence caused by these two variables, we demonstrate the frequency spectrum by varying both signal phase and eccentricity.

High-power side lobe (HPSL): when an eccentricity is set to a large value, in frequency spectrums of 16-EAPM, some side lobes are observed with substantially higher power than other side lobes. Compared to 16QAM, in 16-EAPM, attenuation of such side lobes will cause non-neglectable power loss and waveform distortion. For an easy explanation, we define these distinctive side lobes as high-power side lobes in this paper.

In frequency spectrums generated based on random data of transmitted signals, we have observed that power and number of HPSL increase with the increase of eccentricity. Fig.5 and Fig.6 show frequency spectrums of 16-EAPM generated by varying the eccentricity to four different values respectively, and two types of frequency spectrums have shown similar characteristics. We also notice that centre frequency of all HPSLs equals to odd number of normalized frequency ($3f_c$ and $5f_c$).

According to characteristics of frequency spectrums, 16 Star-EAPM signals are divided into two groups and 16 Square-EAPM signals are divided into three groups. Fig.7 and Fig.8 show frequency spectrums of different groups of signals with eccentricity of 0.9 for 16 Star-EAPM and 16 Square-EAPM, respectively. In both schemes, frequency spectrums generated based on different groups of signals differ slightly in magnitude of HPSL, but same order of HPSL appears at the same eccentricity.

By varying the eccentricity from 0.1 to 0.9 with unit increment of 0.1, the first order of HPSL appears when eccentricity exceeds 0.4, with $3f_c$ as its centre frequency; the second

order of HPSL appears when eccentricity exceeds 0.7, with $5f_c$ as its centre frequency. As an instance, such characteristics of frequency spectrums are demonstrated in Fig.9.
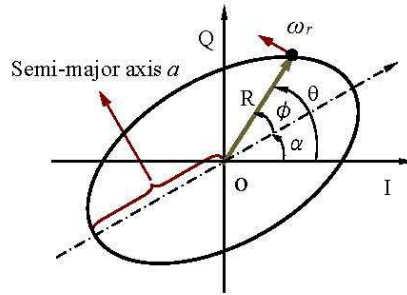

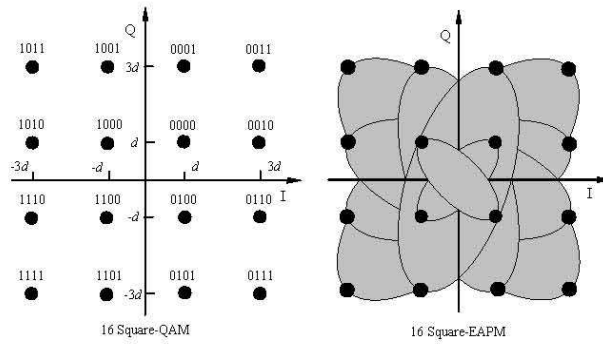Figure 1.   Definitions of variables in an elliptical signal

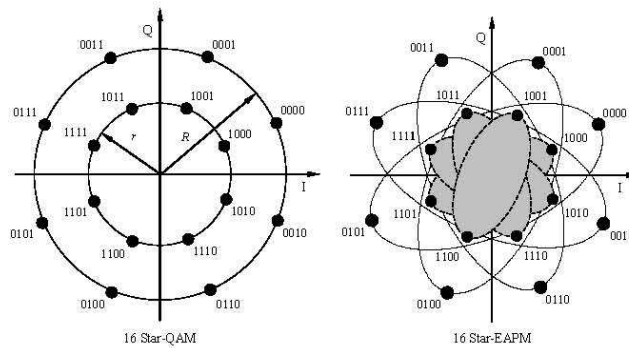Figure 2.   Constellations of 16-EAPM and 16QAM of square mapping

Figure 3.   Constellations of 16-EAPM and 16QAM of Star mapping
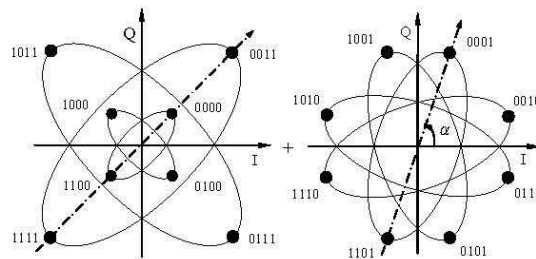

Figure 4.   Decomposed constellation of 16 Square-EAPM
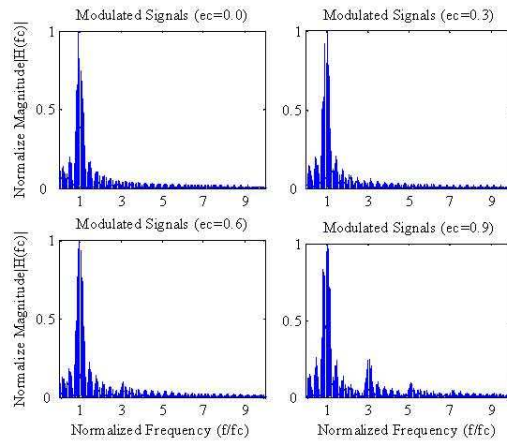
Figure 5. Frequency spectrums of 16 Star-EAPM generated based on random data
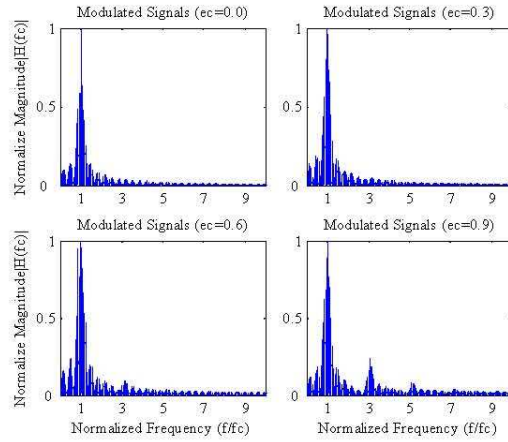

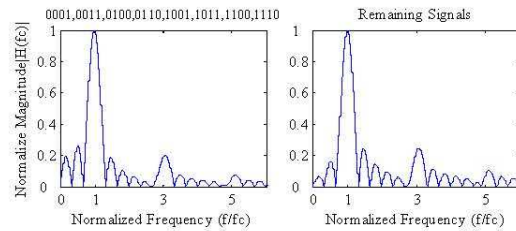Figure 6. Frequency spectrums of 16 Square-EAPM generated based on random data

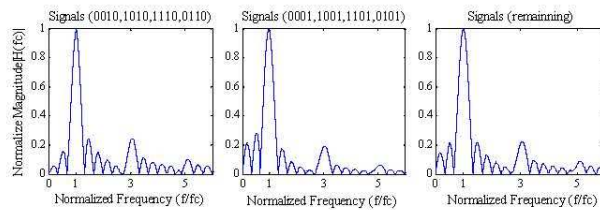Figure 7. Frequency spectrums of 16 Star-EAPM with eccentricity of 0.9

Figure 8. Frequency spectrums of 16 Square-EAPM with eccentricity of 0.9
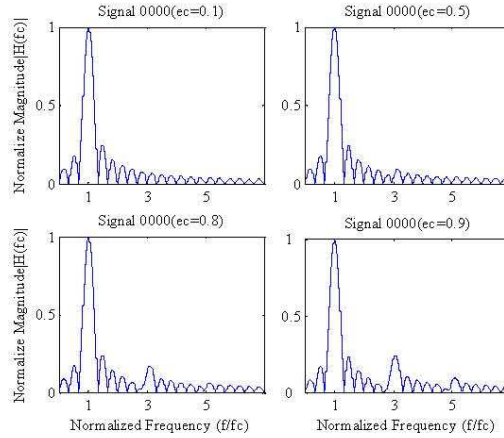
35

Figure 9.   Frequency spectrums of 16 Star-EAPM generated based on a single signal

3. Demodulation of 16-EAPM Signals

Fig.10 shows envelope variation of elliptical carriers with eccentricity of 0.9 in one symbol duration, from which we know that the envelope varies in a duration that equals to half symbol duration. Then by sampling a virtual constellation defined based on ellipses in one symbol duration, achieved samples, i.e., signal components, have different values of envelope. In this case, it is easy to understand that signal components with different envelopes have different levels of noise immunity, and the signal components with peak envelope have better noise immunity than other signal components. To achieve efficient and stable performance, we supposed to detect M-EPSK signals based on the signal components with peak value of envelope in [11] and [12], then dc voltage outputs achieved in I and Q channels respectively are expressed as

$$\begin{cases} V_{I\_M-EPSK(e_c)} = \dfrac{1}{2}a(e_c)\cos\theta_k \\ V_{Q\_M-EPSK(e_c)} = \dfrac{1}{2}a(e_c)\sin\theta_k \end{cases} \tag{13}$$

In [17], for MPSK, dc voltage outputs are given by

$$\begin{cases} V_{I\_MPSK} = \dfrac{1}{2}A\cos\theta_k \\ V_{Q\_MPSK} = \dfrac{1}{2}A\sin\theta_k \end{cases}, \tag{14}$$

in above expressions, both $a(e_c)$ and A denote amplitudes.

Since the derivation of dc voltage outputs in 16-EAPM is similar with that in M-EPSK [11], here, we skip the step and only demonstrate demodulation processing based on dc voltage outputs.

In 16 Star-QAM, the first bit is decided by amplitude detection and the other three bits are decided by phase detection. Similarly, as shown in Fig.21, detection of 16 Star-EAPM signals is also split into two steps: detection of two-level amplitudes combined with phase detection of 8-EPSK signals.

Assuming that in 16 Star-EAPM, dc voltage outputs are extracted from signal components with peak value of envelope, then we have

$$\begin{cases} V_{I\_16\,Star-EAPM\,(e_c)} = \dfrac{1}{2}a_n(e_c)\cos\theta_k \\ V_{Q\_16\,Star-EAPM\,(e_c)} = \dfrac{1}{2}a_n(e_c)\sin\theta_k \end{cases} \qquad (15)$$

In 16 Star-QAM, two dc voltage outputs are given by:

$$\begin{cases} V_{I\_16\,Star-QAM} = \dfrac{1}{2}A_{nI} = \dfrac{1}{2}A_n\cos\theta_k \\ V_{Q\_16\,Star-QAM} = \dfrac{1}{2}A_{nQ} = \dfrac{1}{2}A_n\sin\theta_k \end{cases} \qquad , \qquad (16)$$

in (15) and (16), $a_n(e_c)$ and A_n (n=1,2) denote signal amplitudes.

Without losing a generality, we assume that (6) also exists in 16 Star-EAPM, then ratio of dc voltage output of 16 Star-EAPM_e_c to 16 Star-QAM can be derived and expressed as (for presentation simplicity, 16 Star-EAPM with eccentricity of e_c and 16 Square-EAPM with eccentricity of e_c respectively are denoted by 16 Star-EAPM_e_c and 16 Square-EAPM_e_c).

$$\frac{V_{I\_16\,Star-EAPM(e_c)}}{V_{I\_16\,Star-QAM}} = \frac{V_{Q\_16\,Star-EAPM(e_c)}}{V_{Q\_16\,Star-QAM}} = \frac{a_1(e_c)}{A_1} = \frac{a_2(e_c)}{A_2} \qquad . \qquad (17)$$

Similarly, ratio of dc voltage output of 16 Square-EAPM_e_c to 16 Square-QAM can be derived

$$\frac{V_{I\_16\,Square-EAPM(e_c)}}{V_{I\_16\,Square-QAM}} = \frac{V_{Q\_16\,Square-EAPM(e_c)}}{V_{Q\_16\,Square-QAM}} = \frac{a_n(e_c)}{A_n} \qquad , \qquad (18)$$

where both $a_n(e_c)$ and A_n (n=1,2,3) denote distances between constellation points to the centre point of constellation.
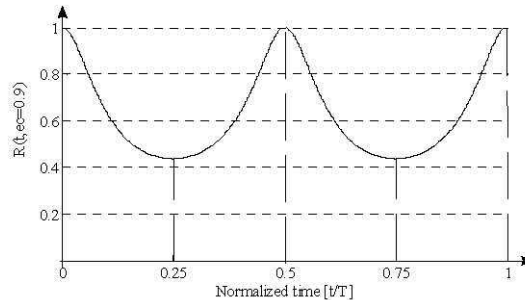

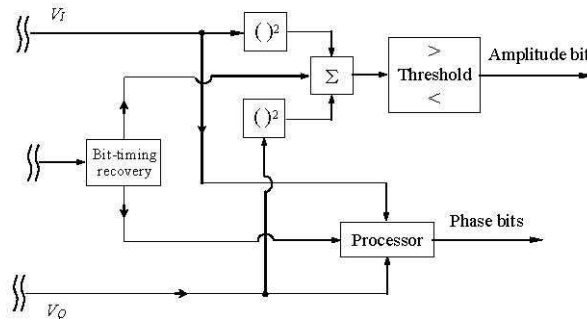Figure 10.   Envelope variation of elliptical carriers

Figure 11.   Receiver functional block diagram for further processing based on dc voltage outputs in 16 Star-EAPM

In constellation of 16 Square-EAPM, four signals in the same quadrant also consist of a small square. Based on this characteristic, constellations of 16 Square-EAPM are divided into four sub-coordinates. In Fig.12, the first subscript number represents quadrant in coordinate and the second subscript number represents quadrant in one of four sub-coordinates. Then for four signals in the same quadrant, difference in both amplitude and phase can be alternated to phase difference in one of sub-coordinates. Thus, signals can be detected by combining phase detection in coordinate and phase detection in sub-coordinate.

In Fig.13, before processor block of 'proc.2' performing logic decision, dc voltage outputs are alternated to I/Q components of signal amplitudes in either of four sub-coordinates, through up-shifting or down-shifting signal levels by a constant value according to their polarities (positive or negative).

As shown in Fig.13, decisions of phase detection in sub-coordinates are made based on results of phase detection in coordinates, so we need to analyze whether or not error detection in coordinate will lead to error detection in sub-coordinate, and consequently cause accumulative error detection. This question is equivalent to whether or not phase detection in coordinate and phase detection in sub-coordinates are independent to each other. Based on Gray code bit mapping and symmetry of the square constellation, analysis of signals in either of four quadrants will reach same conclusion. Without losing a generality, we carry out analysis based on signals in the first quadrant. In coordinate, either the case of noise exceeding $3d$ on either I or Q axis or the case of noise exceeding d on both axes are insignificant. Thus, when considering error detections in coordinate for signals in the first
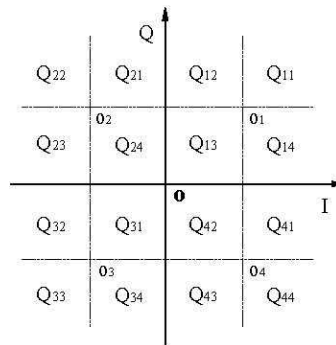

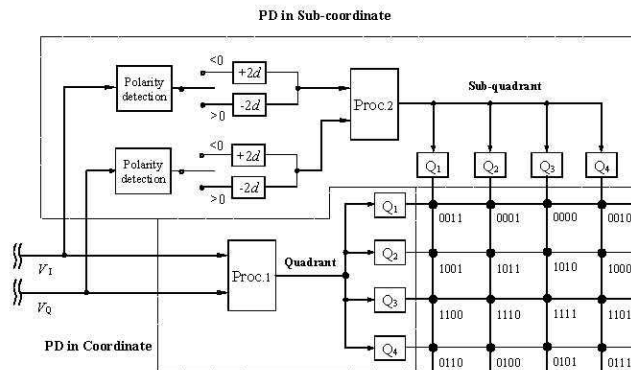Figure 12.   Decision regions of 16 Square-EAPM signals

Figure 13.   Receiver functional block diagrams for further processing based on dc voltage outputs in 16 Square-EAPM

quadrant, it is reasonable to assume that a bit error is most likely to exist between following signal pairs: $Q_{12} \rightarrow Q_{21}$, $Q_{13} \rightarrow Q_{24}$, $Q_{13} \rightarrow Q_{42}$, $Q_{14} \rightarrow Q_{41}$. By referring to Fig.2, we know that the last two digit bits of each pair of signals are same for all above signal pairs, so error detection in coordinate (the first two bits) will not lead to error detection in either of four sub-coordinates (the other two bits). In other words, phase detection in coordinate and phase detection in sub-coordinates are independent to each other with respect to the probability of error detection.

Above analysis on demodulations of 16-EAPM show that the further processing based on dc voltage outputs is a linear process.

Based on fixed signal power, (17) and (18) are directly proportional to eccentricity. In following analysis, we will show that (17) and (18) can approximately but not accurately express the performance comparison results, especially when eccentricity is set to a large value.

4. Derivation of BER Approximations

4.1 An Increment of Decision Radius

In 16 Square-QAM, let d denote decision radius, then from signal constellations we have

$$A_1 = \sqrt{2}d, \quad A_2 = \sqrt{10}d, \quad A_3 = \sqrt{18}d, \tag{19}$$

and A_n (n=1,2,3) is signal amplitude. Then average signal power is calculated by

$$\overline{P}_{16\,Square-QAM} = \frac{d^2}{16}(4 \times 2 + 8 \times 10 + 4 \times 18) = 10d^2. \tag{20}$$

Assuming same decision radius, in 16 Star-QAM,

$$R - r = 2r\sin\frac{\pi}{8} = 2d \Rightarrow \begin{cases} r = A_1 = 2.61d \\ R = A_2 = 4.61d \end{cases}, \tag{21}$$

where definitions of r and R can be referred to (6). Then average signal power equals to

$$\overline{P}_{16\,Star-QAM} = \frac{d^2}{16}(8 \times 2.61^2 + 8 \times 4.61^2) = 14.03d^2. \tag{22}$$

Results derived in (20) and (22) are same with that achieved in [18].

Based on (17) and (18), once $a_n = A_n$ exist between 16-EAPM and 16QAM of same code bit mapping, same decision radius of d can be achieved for all schemes, and in such a case, average signal powers of 16-EAPM are given by

$$\overline{P}_{16\,Square-EAPM} = \frac{1}{16}(4 \times a_1b_1 + 8 \times a_2b_2 + 4 \times a_3b_3) = \frac{1}{4}(a_1^2 + 2a_2^2 + a_3^2)\cdot\sqrt{1-e_c^2} = 10d^2\cdot\sqrt{1-e_c^2}, \tag{23}$$

$$\overline{P}_{16\,Star-EAPM} = \frac{1}{16}(8 \times a_1b_1 + 8 \times a_2b_2) = 14.03d^2\cdot\sqrt{1-e_c^2}. \tag{24}$$

where a_n and b_n (n=1,2,3) are semi-major axis and semi-minor axis of an ellipse, respectively.

Assuming same decision radius, we compare average signal powers for four schemes. Let $k_1(e_c)$ denote ratio of average signal power of 16 Square-EAPM_e_c to 16 Square-QAM, and let $k_2(e_c)$ denote ratio of average signal power of 16 Star-EAPM_e_c to 16 Star-QAM, then

$$k_1(e_c) = k_2(e_c) = \sqrt{1-e_c^2} = k(e_c). \tag{25}$$

Since $k_1(e_c)$ and $k_2(e_c)$ have same value, we use $k(e_c)$ to express the ratio value.

In following evaluations, we assume same average signal power for four schemes, and assume optimum detection with perfect carrier tracking, frequency tracking and symbol synchronization [13], [20].

Let $h(e_c)$ denote ratio of decision radius of 16-EAPM_e_c to 16QAM of same code bit mapping, then according to relationship between bit energy and decision radius, $h(e_c)$ can be derived from (25) as

$$h(e_c) = \frac{d_{16-EAPM(e_c)}}{d_{16QAM}} = \frac{1}{\sqrt{k(e_c)}} = \frac{1}{\sqrt[4]{1-e_c^2}} \qquad (26)$$

From the results we know that based on same average signal power, 16-EAPM can achieve larger decision radius compared to 16QAM of same code bit mapping, and the advantage can be strengthened by increasing eccentricity.

4.2 Comparison of Signal-to-noise Ratio

According to analysis to frequency spectrums of 16-EAPM in sect.2, increase of eccentricity leads to increase on both the power and the number of high-power side lobe (HPSL). Compared to 16QAM, in 16-EAPM, frequency spectrums becomes distinctive when the eccentricity exceeds 0.5, and which may lead to following two effects on decision parameters of performance:

- Increased system noise equivalent bandwidth;
- Increased power loss caused by attenuation of side lobes.

Both effects lead to performance degradation of 16-EAPM.

In 16QAM, relationship of C/N and E_b/N_0 is expressed as:

$$\frac{C}{N} = \frac{\log_2 M \cdot E_b}{N_0} \cdot \frac{1}{B_n T} \qquad , \qquad (27)$$

where T is one symbol duration and B_n is system noise equivalent bandwidth [19].

We use $B_n(e_c)$ to denote optimum value of system noise equivalent bandwidth of 16-EAPM_e_c. Compared to B_n of 16QAM, $B_n(e_c)$ achieves substantial increment when the eccentricity exceeds 0.5. In consequence, compared to 16QAM, in 16-EAPM, extra power loss caused by attenuating HPSLs also becomes substantial. Here we calculate this power loss.

Let P_0, P_n (n=1,2,…) and P_{sum} denote power of main lobe, power of the nth order of HPSL and sum power of all HPSLs, respectively, then

$$P_{sum} = \sum_{j=1}^{n} P_j = P_0 \left[\frac{|H(f_1)|}{|H(f_0)|}\right]^2 + P_0 \left[\frac{|H(f_2)|}{|H(f_0)|}\right]^2 \cdots + P_0 \left[\frac{|H(f_n)|}{|H(f_0)|}\right]^2 = P_0 \sum_{j=1}^{n} \left[\frac{|H(f_j)|}{|H(f_0)|}\right]^2 \qquad , \qquad (28)$$

where $|H(f_n)|$ represents absolute normalized magnitude of the nth order of HPSL. Values of $|H(f_n)|$ can be calculated from frequency spectrums.

Then signal power of 16-EAPM_e_c can be expressed as

$$P_{16-EAPM(e_c)} = P_{Bn(e_c)} + P_{HPSL\_e_c} + P_{rem\_e_c} \qquad , \qquad (29)$$

where $P_{Bn(ec)}$ denotes power of frequency components within bandwidth of $Bn(e_c)$, P_{HPSL_ec} is sum power of all HPSLs calculated by (28), P_{rem_ec} is power of remaining frequency components.

Similarly, for a 16QAM signal, we have

$$P_{16QAM} = P_{Bn} + P_{rem} \qquad , \qquad (30)$$

where P, P_{Bn} and P_{rem} are signal power, power of frequency components within bandwidth of

B_n, and power of remaining frequency components, respectively.

In (30), P_{rem} only consists of small ratio of whole signal power. Similarly, in (29), P_{rem_ec} is also neglectable compared to signal power. Thus, following relationship can be derived from (29) and (30)

$$P_{Bn} \approx P_{Bn(e_c)} + P_{HPSL\_e_c} \,.$$

(31)

Let $\rho(e_c)$ denote the ratio of $P_{Bn(ec)}$ to P_{Bn}, then we can derive

$$\rho(e_c) = \frac{P_{Bn(e_c)}}{P_{Bn}} \approx \frac{P_{Bn(e_c)}}{P_{Bn(e_c)} + P_{HPSL\_e_c}} \,.$$

(32)

Both of P_{Bn} and $P_{Bn(ec)}$ are mainly consisted of mainlobe power. In (32), value of $\rho(e_c)$ will be slightly increased if we substitute P_{Bn} and $P_{Bn(ec)}$ with mainlobe powers of 16QAM and 16-EAPM respectively; however, since this approximate treatment can substantially simplify computation in (32), we calculate $\rho(e_c)$ from (28) by employing the solution. The achieved results for 16-EAPM with eccentricities of 0.8 and 0.9 are shown in below.

For two modulation schemes of square mapping,

$$\rho(e_c = 0.8) = 0.970 \,, \quad \rho(e_c = 0.9) = 0.948 \,;$$

(33)

for two modulation schemes of star mapping,

$$\rho(e_c = 0.8) = 0.972 \,, \quad \rho(e_c = 0.9) = 0.949 \,.$$

(34)

Based on comparison between simulation results and analytical results, we will discuss later in this paper, about the influence of above approximate solution to the derived BER approximations.

Both increments of system noise equivalent bandwidth and power loss of received signals caused by attenuation of HPSLs lead to degradation of signal-to-noise ratio. When making comparison of signal-to-noise ratio between 16QAM and 16-EAPM, we assume same signal bit energy and same noise power spectral density. Let E_b/N_0 and $(E_b/N_0)_{ec}$ denote ratios of bit-energy-to-noise-power-spectral-density of 16QAM and 16-EAPM$\_e_c$ respectively, then relationship between $(E_b/N_0)_{ec}$ and E_b/N_0 is expressed as

$$\left(\frac{E_b}{N_0}\right)_{ec} = \frac{E_b}{N_0} \cdot \frac{\rho(e_c)}{B_n(e_c)T/B_nT} = \frac{E_b}{N_0} \cdot \frac{B_nT}{B_n(e_c)T} \cdot \rho(e_c) \,,$$

(35)

where $Bn(e_c)$ denotes system noise equivalent bandwidth of 16-EAPM$\_e_c$ when using an optimum receiver filter, $\rho(e_c)$ is defined in (32); see other variables in (27).

In 16QAM, $B_nT=1$ when using a matched filter, then (35) can be simplified to

$$\left(\frac{E_b}{N_0}\right)_{ec} = \frac{E_b}{N_0} \cdot \frac{1}{B_n(e_c)T} \cdot \rho(e_c) \,.$$

(36)

By alternating $(E_b/N_0)_{ec}$ to E_b/N_0 according to (36), it enables to compare performance between 16-EAPM and 16QAM of same code bit mapping based on required E_b/N_0.

4.3 BER Approximations

BER approximations of M-QAM of square mapping are generally given by

$$P_B \approx \frac{\overline{n}}{\log_2 M} Q\left(\frac{d}{\sigma}\right) - \left(\frac{\overline{n}}{\log_2 M} Q\left(\frac{d}{\sigma}\right)\right)^2 \,,$$

(37)

where $\bar{n}$ denotes average number of closest signals of each constellation point, and d is decision radius [21].

In 16 Square-QAM, decision radius is given by

$$d = \sqrt{\frac{3\log_2 M \cdot E_b}{2(M-1)}} = \sqrt{\frac{2E_b}{5}} \quad , \tag{38}$$

where E_b denotes bit energy [22].

In 16 Square-EAPM, decision radius is calculated from (26) and (38) as

$$d = h(e_c) \cdot \sqrt{\frac{2E_b}{5}} = \sqrt{\frac{2E_b}{5} \Big/ \sqrt{1-e_c^2}} \quad . \tag{39}$$

Furthermore, in 16-EAPM, instead of E_b/N_0, $(E_b/N_0)_{ec}$ is used. Therefore, BER approximation of 16 Square-EAPM is derived by substituting (36) and (39) to (37)

$$P_B \approx \frac{3}{4} Q\left(\sqrt{\frac{4}{5} \cdot \left(\frac{E_b}{N_0}\right)_{ec} \cdot \frac{1}{\sqrt{1-e_c^2}}} \right) - \left(\frac{3}{4} Q\left(\sqrt{\frac{4}{5} \cdot \left(\frac{E_b}{N_0}\right)_{ec} \cdot \frac{1}{\sqrt{1-e_c^2}}} \right) \right)^2$$

$$= \frac{3}{4} Q\left(\sqrt{\frac{4}{5} \cdot \frac{E_b}{N_0} \cdot \frac{\rho(e_c,\alpha)}{B_n(e_c)T} \cdot \frac{1}{\sqrt{1-e_c^2}}} \right) - \left(\frac{3}{4} Q\left(\sqrt{\frac{4}{5} \cdot \frac{E_b}{N_0} \cdot \frac{\rho(e_c,\alpha)}{B_n(e_c)T} \cdot \frac{1}{\sqrt{1-e_c^2}}} \right) \right)^2 \quad . \tag{40}$$

As for comparison, BER expression of 16 Square-QAM is also shown here [23]

$$P_B = \frac{3}{4} Q\left(\sqrt{\frac{4E_b}{5N_0}} \right) - \left(\frac{3}{4} Q\left(\sqrt{\frac{4E_b}{5N_0}} \right) \right)^2 \quad . \tag{41}$$

Using initial assumption of coherent reception in an AWGN channel, bit error probability of 16 Star-QAM calculated using the signal-space method is given by

$$P_B \approx \frac{1}{4}\left[Q\left(\sqrt{D \cdot \frac{2E_b}{N_0}} \right) + Q\left(\sqrt{E \cdot \frac{2E_b}{N_0}} \right) + Q\left(\sqrt{F \cdot \frac{2E_b}{N_0}} \right) \right] \quad , \tag{42}$$

where

$$D = \frac{8\sin^2(\pi/8)}{1+\beta^2} \quad , \qquad E = \frac{2(\beta-1)^2}{1+\beta^2} \quad , \qquad F = \frac{8\beta^2\sin^2(\pi/8)}{1+\beta^2} \quad , \tag{43}$$

here β denotes optimum ring ratio, then by referring to (6), we have

$$D = 0.284 \,, \quad E = 0.285 \,, \quad F = 0.887 \quad . \tag{44}$$

By substituting (44) to (42), we obtain BER approximation of 16 Star-QAM

$$P_B \approx \frac{1}{2} Q\left(\sqrt{0.57 \cdot \frac{E_b}{N_0}} \right) + \frac{1}{4} Q\left(\sqrt{1.77 \cdot \frac{E_b}{N_0}} \right) \quad , \tag{45}$$

which is consistent with the result shown in [24].

By employing the same principle applied in deriving error probability of 16 Square-EAPM from that of 16 Square-QAM, we derive BER approximation of 16 Star-EAPM from that of 16 Star-QAM, which is given by

$$P_B \approx \frac{1}{2} Q\left(\sqrt{\frac{0.57}{\sqrt{1-e_c^2}} \cdot \left(\frac{E_b}{N_0}\right)_{ec}} \right) + \frac{1}{4} Q\left(\sqrt{\frac{1.77}{\sqrt{1-e_c^2}} \cdot \left(\frac{E_b}{N_0}\right)_{ec}} \right)$$

$$= \frac{1}{2} Q\left(\sqrt{\frac{0.57}{\sqrt{1-e_c^2}} \cdot \frac{E_b}{N_0} \cdot \frac{\rho(e_c)}{B_n(e_c)T}} \right) + \frac{1}{4} Q\left(\sqrt{\frac{1.77}{\sqrt{1-e_c^2}} \cdot \frac{E_b}{N_0} \cdot \frac{\rho(e_c)}{B_n(e_c)T}} \right) \quad . \tag{46}$$

5. Comparison and Discussion

In the interest of verifying correctness and accuracy of the derived BER approximations, we carry out simulations to calculate error probability of 16-EAPM with large eccentricities, and then compare the analytical results with simulation results.

In simulations, demodulation methods illustrated in Sect.3 are employed. Main simulation parameters are defined and shown in Table 1. Two types of 16-EAPM have shown efficient performance based on same simulation parameters. In addition, elliptical filters defined in Table 1 have same bandwidth with the one used in 8-EPSK in [11].

In (40) and (46), values of $\rho(e_c)$ can be approximately calculated using (33) and (34), then once values of $B_n(e_c)T$ are known, theoretical error probability of 16-EAPM can be computed. However, the optimum filter should be designed based on trade-offs between waveform distortion and signal-to-noise ratio in terms of error performance, and based on trade-offs between power efficiency and spectrum efficiency. Thus, definition and design of the optimum filter consist of complex works, and which is left for our future study. Since efficient performance are achieved in simulations, we calculate $B_n(e_c)T$ based on parameters shown in Table 1 and apply the achieved value to compute theoretical error probability.

According to Table 1, $B_n(e_c)T$ equals to 1.19. By substituting $B_n(e_c)T$=1.19 and (33) to (40), we derive BER approximation of 16 Square-EAPM_0.9, which is given by

$$P_B \approx \frac{3}{4}Q\left(\sqrt{\frac{4}{5}\frac{E_b}{N_0}\cdot 1.8315}\right) - \left(\frac{3}{4}Q\left(\sqrt{\frac{4}{5}\frac{E_b}{N_0}\cdot 1.8315}\right)\right)^2 \quad , \tag{47}$$

Similarly, we derive BER approximations of 16 Square-EAPM_0.8, 16 Star-EAPM_0.8 and 16 Star-EAPM_0.9 and show the results in below:

$$P_B \approx \frac{3}{4}Q\left(\sqrt{\frac{4}{5}\frac{E_b}{N_0}\cdot 1.3627}\right) - \left(\frac{3}{4}Q\left(\sqrt{\frac{4}{5}\frac{E_b}{N_0}\cdot 1.3627}\right)\right)^2 \quad , \tag{48}$$

$$P_B \approx \frac{1}{2}Q\left(\sqrt{0.57\cdot\frac{E_b}{N_0}\cdot 1.3627}\right) + \frac{1}{4}Q\left(\sqrt{1.77\cdot\frac{E_b}{N_0}\cdot 1.3627}\right) \quad , \tag{49}$$

$$P_B \approx \frac{1}{2}Q\left(\sqrt{0.57\cdot\frac{E_b}{N_0}\cdot 1.8315}\right) + \frac{1}{4}Q\left(\sqrt{1.77\cdot\frac{E_b}{N_0}\cdot 1.8315}\right) \quad . \tag{50}$$

In Fig.14 and Fig.15, we compare analytical results, which are calculated using (47)~(50), with simulation results achieved based on parameters defined in Table 1. Error probabilities of two types of 16QAM are calculated using (41) and (45), respectively. For both types of 16-EAPM, simulation results are slightly worse than analytical results. This degradation of E_b/N_0 approximates to 0.29dB for 16 Square-EAPM_0.9 and approximates to 0.26dB for 16 Star-EAPM_0.9; and the degradations approximate to 0.12dB and 0.1dB for 16 Square-QAM_0.8 and 16 Star-EAPM_0.8, respectively.

Table 1: Simulation Parameters

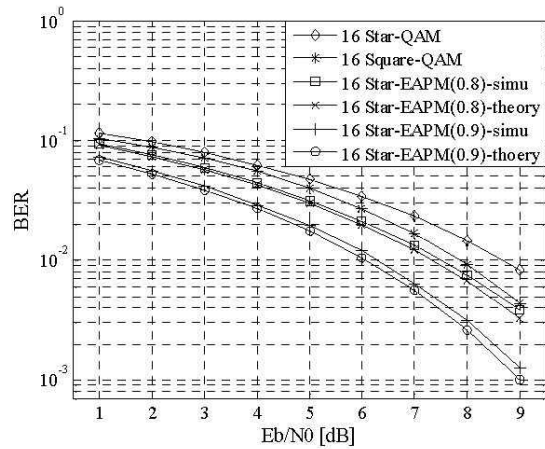| Transmission rate	256 [k symbol/s]	Passband ripple	3 dB
Carrier frequency	f_c=768 [kHz]	Stopband attenuation	60 dB
Cut-off frequency	f_{c1}=648, f_{c2}=953 [kHz]	Sampling frequency	f_s=30.72 [MHz]
Passband edge frequency	f_{a1}=623, f_{a2}=978 [kHz]	order	8

Figure 14.   BER comparison of analytical results and simulation results
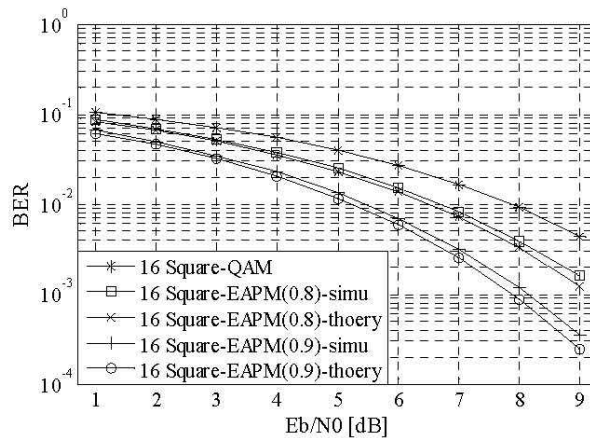

Figure 15.   BER comparison of analytical results and simulation results

We think it is waveform filtering that has caused above performance degradation in simulation results compared to analytical results in 16-EAPM. When eccentricities are set to large values, waveform filtering attenuates high power side lobes, attenuation of such side lobes then causes waveform distortion and lead to increase of $k(e_c)$ in (25). Consequently, waveform filtering degrades the noise performance. Since this influence hasn't been taken into account in deriving BER approximations, theoretical BER approximations derived in (40) and (46) can only be closely approached, but can not be perfectly realized.

Based on the analytical results, 16-EAPM_0.8 and 16-EAPM_0.9 can achieve advantage of 1.344dB and 2.628dB E_b/N_0 over 16QAM of same code bit mapping respectively, at the expense of reducing bandwidth efficiency around 16.0%; 16 Star-EAPM_0.8 can improve error performance compared to 16 Square-QAM, and 16 Star-EAPM_0.9 has better error performance than 16 Square-EAPM_0.8.

6. Conclusion

In this paper, we investigate a new solution of realizing combined amplitude and phase modulation by employing elliptical signals. Two proposed 16-ary modulation schemes are

defined as 16-ary Elliptical Amplitude Phase Modulation (16-EAPM) of square mapping (16 Square-EAPM) and star mapping (16 Star-EAPM). Compared to 16QAM, in 16-EAPM of same code bit mapping, decision radius and occupied bandwidth are increased by increasing eccentricity. Increase of decision radius contributes toward improving error performance, while increase of occupied bandwidth degrades error performance. According to our evaluations, when increasing eccentricity, increment of decision radius is more substantial than increment of occupied bandwidth with respect to their effects to error performance. Thus, 16-EAPM can achieve better noise performance than 16QAM of same code bit mapping at the expense of decreasing spectrum efficiency. Evaluation results also show that in 16-EAPM, error performance is directly proportional to eccentricity while spectrum efficiency is inversely proportional to eccentricity. This provides two schemes with good flexibility to make tradeoffs between power efficiency and bandwidth efficiency by varying eccentricity. BER approximations have been derived for 16-EAPM and which are in agreement with simulation results.

Simulation-based evaluations have shown that BER approximations derived for 16-EAPM can not be perfectly realized when eccentricity is set to a large value. In applications, characteristics of filters combined with corresponding system noise equivalent bandwidth will decide how close achieved performance can approach theoretical results. In future works, definition and design of the optimum filter and mathematical derivation of corresponding optimum value of system noise equivalent bandwidth need to be studied, so as to realize efficient trade-offs between power efficiency and bandwidth efficiency. In addition, we also need to investigate carrier tracking problems that 16-EAPM will encounter in mobile fading channels.

References

[1] P.M.fortune, L.Hanzo and R.steele, "On the computation of 16-QAM and 64-QAM performance in Rayleigh-fading channel," *IEICE Trans. on Comm.*, vol.E75-B, pp.466-475, June 1992.

[2] F.Adachi, M.Sawahashi, "Performance Analysis of Various 16 Level Modulation Schemes under Rayleigh Fading," *Electronics Letters*, Vol.28, No.17, 13th August 1992, pp.1597-1581.

[3] Y.C.Chow, A.R.Nix and J.P.McGeehan, "Analysis of 16-APSK Modulation in AWGN and Rayleigh Fading Channel," *Electronics Letters*, Vol.28, No.17, 13th Aug. 1992, pp.1608-1610.

[4] S.Sampei and T.Sunaga, "Rayleigh Fading Compensation for QAM in Land Mobile Communication," *IEEE Trans. Veh. Technol.*, Vol.42, No.42, May. 1993, pp.137-147.

[5] Y.C.Chow, A.R.Nix and J.P.McGeehan, "Error Analysis for circular 16-DAPSK in Frequency-Selective Rayleigh Fading Channels with Diversity Reception," *Electronics Letters*, Vol.30, No.24, 1994, pp.2006-2007.

[6] D.Subasinghe-Dias and K.Feher, "A Coded 16QAM Scheme for Fast Fading Mobile Radio Channels," *IEEE Trans. on Comm.*, Vol.43, May.1995, pp.1906-1916.

[7] F.Adachi, "Error Rate Analysis of Differentially Detected 16APSK Under Rician Fading," *IEEE Trans. Veh. Technol.*, Vol.45, No.1, Feb. 1996, pp.1-11.

[8] Xiaodai Dong, Tjeng Thiang Tjhung, F.Adachi, "Error Probability Analysis for 16 Star-QAM in Frequency-Selective Rician Fading with Diversity Reception," *IEEE Trans. Veh. Technol.*, Vol.47, No.3, August1998, pp.924-935.

[9] Eiji Okamoto, Huan-bang Li and Tetsushi Ikegami "Rayleigh Fading Compensation for 16QAM Using FFT," *IEEE Trans. Veh. Technol.*, Vol.48, No.5, Sep. 1999, pp.1626-1633.

[10] Chunyi Song, S.Shimamoto, "Proposal and Evaluation of 8−ary Elliptical Phase Shift Keying," *Proc. IEEE International Conference on Communications* 2005. ICC 2005. Vol.1, Page(s):598 – 602, May 2005.

[11] Chunyi Song and S.Shimamoto, "Improvement on Power Efficiency of M-EPSK by employing Elliptical Signals," *Proc. IEEE Wireless Communications and Networking Conference* 2006, WCNC 2006. Vol.4, page(s): 1921-1926. Apr. 2006.

[12] Yantao Qiao, Chunyi Song and Shimamoto, S., "Rate 2/3 Trellis-Coded 8-ary Elliptical Phase Shift Keying Modulation", *Proc. IEEE 4th International Symposium on Wireless Communication Systems (ISWCS)*, 2007. Page(s): 161 - 165, Oct. 2007.

[13] Chunyi Song, Shimamoto, S., "A Proposal of an Efficient Timing Recovery Algorithm for 4-ary Elliptical

Phase Shift Keying", *Proc. Future generation communication and networking* 2007 (FGCN'07), Vol.1, Page(s):296 – 300, Dec. 2007.

[14] Chunyi Song and S.Shimamoto, "Effects of Eccentricity on Performance of M-ary Elliptical Phase Shift Keying (M=4,8)," *Proc. IEEE WCNC* 2008, page(s): 1945-1949, Apr. 2008.

[15] Theodore.S.Rappaport, *Wireless Communications – Principles and Practice* (Second Edition), Prentice Hall PTR, 2002.

[16] John G. Proakis, M. Salehi, *Contemporary Communication Systems Using MATLAB,* Brooks/Cole, a division of Thomson Learning, USA, 2000.

[17] Paul H. Yang, *Electronic Communication Techniques* (Fourth Edition), Prentice Hall, 1999.

[18] B.P.Lathi, *Modern Digital and Analog Communication System*, Oxford University Press, Oxford, 1998.

[19] B. Sklar, *Digital Communications – Fundamentals and Applications* (Second Edition), Prentice Hall PTR, 2002.

[20] U. Mengali and A. N. D'Andrea, *Synchronization Techniques for Digital Receivers*. New York: Plenum Press, 1997

[21] Jianhua Lu, K.B.Letaief, Justin C-I Chuang and Ming L. Liou, "16QAM and M-QAM BER Computation Using Signal-Space Concepts," *IEEE Trans. on Comm.*, Vol.47, No.2, Feb.1999, pp.181-184.

[22] Alister Burr, *Modulation and Coding for Wireless Communications*, Prentice Hall, 2001.

[23] Andrea Goldsmith, *Wireless Communication*, Cambridge University Press, 2005.

[24] BENEDETTO S., BIGLIERI E. and CASTELLANI V., *Digital Transmission Theory*, Prentice-Hall International Edition, 1987.

Authors
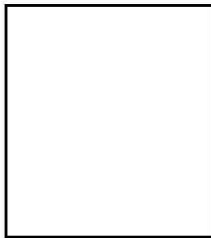
Chunyi SONG received B.E. degree from Jilin University, Jilin, China in 2003. He was special research student during Oct.2001-Mar.2003 in Waseda University, supported by Japanese government scholarship. He completed his doctor course in Waseda University in 2007, and joined Global Information and Telecommunication Institute (GITI) of Waseda University from April 2007, where he currently is doing as a Research Associate. His main research interest includes modulation, coding theory, ad hoc network and cognitive radio. He is a member of IEEE and IEICE Japan.